Journal Pre-proof

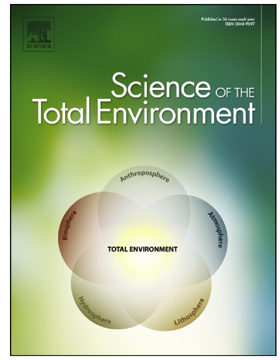

Modelling the impact of past and future climate scenarios on streamflow in a highly mountainous watershed: A case study in the West Seti River Basin, Nepal

Binod Bhatta, Sangam Shrestha, Pallav K. Shrestha, Rocky Talchabhadel

PII: S0048-9697(20)33677-9

DOI: https://doi.org/10.1016/j.scitotenv.2020.140156

Reference: STOTEN 140156

To appear in: *Science of the Total Environment*

Received date: 24 December 2019

Revised date: 9 June 2020

Accepted date: 10 June 2020

Modelling the Impact of Past and Future Climate Scenarios on Streamflow in a Highly Mountainous Watershed: A Case Study in the West Seti River Basin, Nepal

Binod Bhatta, Sangam Shrestha, Pallav K. Shrestha, Rocky Talchabhadel

[1]Water Engineering and Management, School of Engineering and Technology, Asian Institute of Technology, P.O. Box 4, Klong Luang, Pathum Thani 12120, Thailand

[2]Helmholtz Centre for Environmental Research GmbH - UFZ, Permoserstraße 15, 04318 Leipzig, Germany

[3]Disaster Prevention Research Institute, Kyoto University, Higashino Kuchi, Shimomisu, Yoko-oji, Fushimi-ku, Kyoto 612-8235, Japan

[4]Stockholm Environment Institute (SEI), Asia Centre, Bangkok, Thailand

Corresponding Author:

*Binod Bhatta

binodbhatta40@gmail.com

Abstract

Hydrological model parameters are important during representation of the hydrological characteristics of a watershed. The West Seti River Basin (WSRB), a prominent Himalayan Basin of Nepal, is a major source of fresh water in the western region of the country. We used the Soil and Water Assessment Tool (SWAT) for hydrological modelling and identified the most sensitive hydrological parameters, while the Sequential Uncertainty Fitting (SUFI-2) technique was employed for model calibration. The model was calibrated for the study period (1999–2005) with a three-year warm-up period (1996–1998). Subsequently, it was validated for three years (2006–2008). The results show that the large number of Hydrological Response Units (HRUs) for model simulation took a considerable time, without improving the performance statistics. Importantly, significant improvements were observed during both calibration and validation periods when elevation bands (EBs) were taken into consideration. The p-factor, r-factor, coefficient of determination (R^2), Nash–Sutcliffe efficiency (NSE), percent bias (PBIAS), Root mean square error (RMSE)-observations, and standard deviation (STDEV) ratio (RSR) were used to measure the performance between observed and simulated values. The values of p-factor, r-factor, R^2, NSE, PBIAS, and RSR during the calibration were 0.82, 0.80, 0.84, 0.82, 7.2, and 0.42, respectively, whereas during validation they were 0.79, 0.72, 0.83, 0.82, 11.8, and 0.42, respectively. The calibrated model was then used to assess the anticipated river discharge. This study used four regional climate models (RCMs) for precipitation and six for temperature, together with their arithmetical average as multi-model ensembles (MMEs) under two representative concentration pathways (RCPs). We analysed the changes in precipitation, temperature, and river discharge for three future time frames: Future1 (F1: 2020–2044), Future2 (F2: 2045–2069), and Future3 (F3: 2075–2099) with respect to the baseline (1996–2005). The magnitude of changes varied according to the different climate models and warming scenarios. In general, the MMEs showed slightly increasing precipitation (higher during the F2 period), significantly increasing temperature (continuous rising trend), and moderately increasing river discharge (higher during the F2 period). Information such as the anticipated shift in the flow duration curve may be helpful to stakeholders across different water sectors for effective water resource management in the future. From the modelling perspective, the results show greater significance for EBs than HRUs during the modelling of high mountain basins with SWAT. This take-home message would be useful to hydrologists and other stakeholders in evaluating different scenarios over a short duration, without iteratively spending higher computational time.

Keywords: West Seti River Basin, Climate change, Hydrological modelling, Soil and Water Assessment Tool

1. Introduction

The hydrological cycle has a strong link with both the surface and subsurface processes of the earth. The SWAT is widely acknowledged as a robust tool for interdisciplinary watershed-modelling and is a physically-based semi-distributed model (Abbaspour et al., 2015). According to Gassman & Yingkuan (2015), SWAT is a suitable model for predicting land management, the long-term impact on sediment, agricultural yield, and streamflow simulation based on their study conducted in a large and very complex watershed, with varying land use, management practices and soil conditions. Krysanova & White (2015) investigated the performance of various models including SWAT, the Dynamic Watershed Simulation Model (DWSM), and Hydrological Simulation Program-Fortran (HSPF). Their study showed SWAT to be an extremely useful tool in agricultural watersheds to simulate streamflow. However, SWAT is not recommended for use in extreme hydrological events like floods. The SWAT model has been extensively used in various countries for discharge prediction (Bajracharya et al., 2018; Lenderink et al., 2007; Shrestha et al., 2018; Khadka et al., 2014; Abbaspour et al., 2015).

Hydrological models contain uncertainty for various reasons including poor input data quality or/and the simplification of complex physical processes with underlying assumptions and limitations. Therefore, it is necessary to calibrate the models to significantly decrease the chances of uncertainty in predictions (Chaibou et al., 2016; Croton et al., 2016). By implementing sensitivity and uncertainty analysis, the parameterisation and calibration of hydrological models can be examined (Refsgaard, 1997). Uncertainty is associated with several factors including input-output parameters and model structure. Therefore, predictions for uncertainty must be in an acceptable range (Shen et al., 2012). A detailed explanation of different sources and types of uncertainty can be found in Yang et al. (2008).

In order to verify the applicability of SWAT, it is a routine step to conduct careful calibration followed by validation (Arnold et al., 2012). Generally, the performance measures are examined using graphical and statistical methods. The performance evaluation range may vary from satisfactory to very good, corresponding to the quantitative threshold for different performance indicators (Moriasi et al., 2007). After ensuring its reliability, the model is then deemed fit to simulate all future conditions (Zhang et al., 2015) or different scenarios.

Generalised Likelihood Uncertainty Estimation (GLUE), SUFI-2, Parameter solutions (ParaSol), and Markov Chain Monte Carlo (MCMC) are the four most commonly-used sensitivity analyses and optimisation algorithms for this model. These algorithms assist in determining the uncertainty in SWAT predictions (Yang et al., 2008). The SWAT-CUP procedure connects all the aforementioned algorithms to the SWAT model, thereby enabling uncertainty and sensitivity analysis. Wu & Chen (2015) utilised ParaSol, GLUE, and SUFI-2 wherein they assessed the applicability and performance of SWAT to predict streamflow in the Lake Tana Basin. Shrestha et al. (2018) conducted an uncertainty analysis and model calibration of SWAT using SUFI-2 to estimate nitrate nitrogen and runoff in the Songkhram River Basin in Thailand. The SUFI-2 algorithm consists of statistical and graphical performance measures to evaluate the robustness of a model. Yang et al. (2008) reported that the SUFI-2 algorithm must have a minimum number of simulations to make it easier to attain high-quality uncertainty analysis and calibration.

The Karnali River, one of the main rivers in Western Nepal, drains almost one-third of the country's catchment. Only a few studies have been carried out in the Karnali River and its tributaries (e.g. Gladfelter 2018; Mishra et al., 2018; Liu et al., 2018; Smith et al., 2017; Dhami et al., 2018; Shiwakoti, 2017). None of the previous studies, to the best of our knowledge, have evaluated the influence of hydrological parameters on runoff simulation, considering computational time, in the western region of Nepal. The West Seti is a major tributary of the Karnali River and has great importance in fulfilling the food security and energy demand of the area. In addition, the West Seti River Basin (WSRB) is one of the top four most vulnerable basins in Nepal when it comes to climate change. Karki (2012) analysed the uncertainty in the WSRB using SWAT and underscored the importance of a monthly or seasonal performance check. Gurung et al. (2013, 2015) employed SWAT in the WSRB to simulate the water balance in different cropping patterns under current and future climates. Pradhan et al. (2019) assessed the performance of SWAT and Artificial Neural Network (ANN) models in three different river basins (including the WSRB) and confirmed the applicability of SWAT in the WSRB.

Similarly, a few available studies have focused on model input structures and their performances in Nepalese watersheds. For instance, Gautam et al. (2019) assessed the impact of digital elevation model (DEM) source, resolution, and area threshold values on the SWAT-generated stream network and streamflow in two different catchments of Nepal. Their study highlights the assumption that the SWAT model performance improvement with DEM resolution does not hold true. However, Gautam et al. (2019) suggested using a higher resolution DEM (30 m or finer) to achieve the best model performance based on the temporal sensitivity of the runoff. Bhatta et al. (2019) assessed the SWAT model performance under different scenarios based on drainage area (DA) threshold, sub-basins (SBs), HRUs, and EBs, paying careful attention to computational time over the eastern Himalayan region of Nepal. In general, upon the creation of a large number of SBs and HRUs, the model performs comparatively better, although it consumes expensive computational time. The modelling becomes more complex when the topography and climate are highly heterogeneous.

There is a huge gap in the unravelling of issues related to model performance in the western region of the country. The country's climatic condition in the western region is quite different from eastern Nepal, especially during the winter season (snowfall at higher altitude) due to the dominance of westerly disturbance (Talchabhadel et al., 2018). The SWAT model is equally applicable in snow-dominated basins (Azmat et Al., 2018; Shrestha and Wang, 2018; Dhami et al., 2018; Pradhanang et al., 2011). Spatial variation in the accumulation and melting of snow could be replicated in the model by sub-dividing the SB into different zones based upon elevation (Shrestha et al., 2017; Pradhanang et al., 2011). The model allows the SBs to be sub-divided into a maximum of ten EBs. Pradhanang et al. (2011) examined the effects of parameterising the SWAT snowmelt sub-model using a number of EBs for comparison measured snow and streamflow. They found that a snow configuration choice greater than three EBs had little effect on the SWAT simulation of streamflow in the Cannonsville Watershed, USA. Therefore, in circumstances where observation-based snow data is lacking, the selection of EBs is also crucial.

It is equally important to understand the projected impact of climate change on the hydrological regime especially in the Himalayan region (Singh & Bengtsson, 2004) for sustainable water resources management (Nepal, 2016). Numerous studies have been conducted to assess the impact of climate change on various disciplines including water resources management using different models on the global (Alcamo et al., 2003, 2007; Hagemann et al., 2013; Hanasaki et al., 2013; Hirabayashi et al., 2008, 2013), regional (Immerzeel et al., 2010, 2013; Piman et al., 2015; Portoghese et al., 2015), national (Chaulagain, 2006; Talchabhadel & Karki, 2019) and local scale (Agarwal et al., 2015; Aryal et al., 2018; Bhatta et al., 2019; Dahal et al., 2016; Gautam et al., 2019; Gurung et al., 2015; Mishra et al., 2018; Nepal 2016; Pandey et al., 2019).

In a Himalayan river basin like the WSRB, an unequivocal, accelerating, warming trend could significantly alter the hydrological regime (Bajracharya et al., 2018).

There are two objectives to our study. Firstly, to analyse the model behaviour by setting it against a range of modelling scenarios, emphasising the treatment complexities related to topography and climate. The output of this objective is to construct a model with optimum computational time and model performance. The second objective is to apply the model for climate change impact assessment. The model setup using the best “performance-and-runtime” from objective one was fed with different climate models and their ensembles (McSweeney et al., 2015) under two warming scenarios (RCP 4.5, a medium stabilising scenario and RCP 8.5, a very high emission scenario) until the end of 2100. Though the current application of the model is limited to an impact assessment of climate change, we believe researchers and practitioners can benefit from this study since it provides a more detailed assessment of adaptation measures in mountainous environments.

This paper is organised as follows: The study area is discussed in section 2, together with a description of meteorological data (observed and projected), and other relevant data. The entire methodology of this study is discussed in section 3. The results and relevant discussions are presented in section 4, while section 5 concludes the study.

2. Study Area and Data Collection

2.1 Study area

Located in the far western region of Nepal, the WSRB is an important source of fresh water in the region (**Fig. 1**). According to existing studies, the WSRB is the most vulnerable watershed of all the 135 in Nepal (Maharjan, 2012). In recent years, the WSRB has come under even greater scrutiny due to a 750 MW hydropower project being proposed by the Government of Nepal

(GoN, 2018). West Seti is one of the major tributaries of the Karnali River (507 km); the longest river in Nepal. The West Seti River originates from the glaciers and snowfields around the twin peaks of Nampa and Api in the main Himalayas, facing towards the South. The area lies within the longitudes 80° 35' - 81°36' and latitudes 29° 02' - 29° 41'. The catchment area of the WSRB at Gopaghat is 4,342 km^2. As with most of the Himalayan basins in Nepal, the WSRB has large elevation, ranging from 610 m asl (above sea level) to 7,019 m asl. A major part of this area (about 63.26%) is forest, with 28.17% agricultural land (ICIMOD, 2010).

Precipitation in the study area is dominated by summer monsoon, which starts in June and lasts until September. Climatic variations (temperate to polar) are observed with higher altitudes located high in the Himalayas (Karki et al., 2016). Average rainfall of 1921 mm was recorded in the study area from 1996 to 2008, at least 75% of which occurred during the monsoon. During the same period, the minimum temperature in the area varied from -23.4 to +31.3 °C with the maximum temperature varying from -17.3 to +46.7 °C. Gurung et al. (2015) reported that on average, the nights have become colder and the days hotter in this region.

2.2 Data collection

Meteorological forcings, streamflow gauges, land use/land cover (LULC), DEM, and soil data were collected for this study and are briefly described here. For DEM, the Advanced Spaceborne Thermal Emission and Reflection Radiometer Global DEM (ASTER GDEM) of 30 m resolution was used, retrieved from https://tahoe.usgs.gov/DEM.html. The DEM was used to delineate the watershed and generate the river stream. The land use map of the WSRB, with a spatial resolution of 1:25,000 was obtained from the Department of Survey, Nepal. Each LULC type is described in brief in **Table 1**, along with descriptions of each class. The most prominent land cover is forest. Urban coverage in the region is insignificant, comprising a few scattered cities. The LULC consists of mixed forest, pasture, barren land, water body, range-brush, agricultural land, and snow/glacier. The soil data was obtained from the Soil and Terrain database (SOTER) website (https://www.isric.org/explore/soter) on a scale of 1:1,000,000, with the WSRB containing eight types (**Table 1**). Hydrological and precipitation data was collected from the Department of Hydrology and Meteorology (DHM). **Table 2** shows the duration and sources of the collected hydro-meteorological data.

Fig. 1.

Table 1

Fig. 2

Table 2

Three future time periods are considered in this study: F1 (2020–2044), F2 (2045–2069), and F3 (2075–2099). We used six RCMs, individual members of the Conformal-Cubic Atmospheric Model (CCAM). The CCAM is a popular Coordinated Regional Climate Downscaling Experiment (CORDEX) for South Asia RCMs, downscaled using different GCM forcings (**Table 3**) at a horizontal resolution of 0.44^{o} (~50 km). The projected data was downloaded from the Centre for Climate Change Research, Indian Institute of Tropical Meteorology (CCCR-IITM, a nodal agency for coordinating CORDEX modelling activity in South Asia). Linear scaling (LS) was employed for bias correcting the projected data. Even though LS is the simplest bias correction method, it is equally effective for assessing water resources of coarser temporal resolution compared to more complex bias correction methods (Shrestha et al., 2017). In LS, the average monthly correction factors were determined for both climate variables (i.e. precipitation and temperature) with reference to observed climate data. The monthly correction factors were then applied in additional (or multiplication) form to obtain the bias-corrected temperature (precipitation).

Table 3

3. Research Methodology

In this study, 18 SWAT models were developed under different scenarios, considering the DA threshold, population of HRU, and population of EB. Calibration and validation were performed for all models using the SUFI-2 algorithm. The calibration runtime varied, depending on the number of SBs and HRUs. Meteorological forcings were kept constant while HRUs, SBs, and EBs were treated as variables to develop the modelling scenarios, and the time required for each modelling scenario compared. **Fig. 3** illustrates the overall methodology applied. After calibration and validation, future bias-corrected climate data in different climate scenarios was fed into the model to analyse the projected river discharge.

Fig.3

3.1 **SWAT modelling**

The SWAT is a physically-based semi-distributed continuous hydrological model (Arnold et al., 2012) developed by the USDA (United States Department of Agriculture). Please refer to Gassman et al. (2007) for a detailed description of the historical development, application, and future research direction of the SWAT model. The major model components of SWAT comprise weather, hydrology, soil properties, plant growth, nutrients, pesticides, bacteria and pathogens, and land management (Arnold et al., 2012). The model can be used to simulate and predict water quality/quantity, soil erosion, sediment yield, impacts of land use/cropping pattern change, and so on. This study employed the SWAT model to simulate the historical river discharge. The validated model was then used to make predictions under changing climate. Theoretical information on SWAT is available at https://swat.tamu.edu/media/99192/swat2009-theory.pdf.

3.2 The SUFI-2 algorithm in SWAT-CUP

The SWAT-CUP is a complementary tool for facilitating sensitivity analysis, calibration, validation, and uncertainty analysis of the SWAT models. Of the various procedures available, the SUFI-2 is arguably the most popular algorithm inside SWAT-CUP. In the SUFI-2, the uncertainty in parameters accounts for uncertainty in the conceptual model, such as from driving variables, measured data, and parameters (Abbaspour et al., 2015). The 95% range of uncertainty (95PPU) is calculated at the 97.5% and 2.5% levels of cumulative distribution. The output variable is obtained using Latin hypercube sampling after disallowing 5% of poor simulations that cannot be taken into account (Abbaspour, 2007). Detailed information on the conceptual basis of the SUFI-2 uncertainty analysis routine is available in Abbaspour et al. (2007). The r-factor and p-factor are used to determine the strength of model calibration (Arnold et al., 2012). The p-factor value varies from 0 to 1 and the r-factor from 0 to infinity. For the p-value, the highest value (1) indicates a 100% match between the observations and simulated data. Its lowest value (0) represents a higher chance of uncertainty in model outputs (Setegn et al., 2010). The p-factor provides an answer to “What percentage of measured data is covered in the envelope of the 95PPU?” It also accounts for all uncertainties associated with the SWAT model. On other hand, the r-factor represents the average thickness of the 95PPU band. To obtain less uncertainty, a lower r-factor value is required (Abbaspour et al., 2015). Both p and r-factors need to be balanced since a higher p-factor value is obtained through a greater r-factor value. Further details of the SUFI-2 are available in the SWAT-CUP user manual (Abbaspour, 2011).

3.3 Performance metrics

Five metrics, namely PBIAS, NSE, R^2, r-factor, and p-factor are employed for evaluating the performance of model results. The R^2 (Eq. 1) estimates the combined dispersion against a single dispersion of the observed and simulated series (Krause et al., 2005). The NSE is a measure for best fit and ranges from (-∞) to (1). The optimal value of the NSE is (1), calculated using Eq. 2.

$$\mathrm{R}^2 = (\frac{(\sum(X_i - X_{avg})(Y_i - Y_{avg}))^2}{\sum(X_i - X_{avg})^2 \sum(Y_i - Y_{avg})^2}, \qquad (1)$$

$$\mathrm{NSE} = 1 - \frac{\sum(X_i - Y_i)^2}{\sum(X_i - X_{avg})^2}, \qquad (2)$$

$$\mathrm{PBIAS} = 100\,(\frac{\sum Y_i - \sum X_i}{\sum X_i}) \qquad (3)$$

$$\mathrm{RSR} = \frac{RMSE}{STDEV_{obs}}\,(\frac{\sqrt{\sum_{i=1}^{n}\left(X_i^{obs} - Y_i^{sim}\right)^2}}{\sqrt{\sum_{i=1}^{n}\left(X_i^{obs} - X_i^{mean}\right)^2}}) \qquad (4)$$

where, X_i represents the measured values, X_{avg} represents the mean of measured values, Y_i represents the simulated values, and Y_{avg} represents the average simulated values. The PBIAS (Eq. 3) is arguably the most commonly-used indicator for quantifying errors in water balance. Additionally, it also indicates poor performance in a model when deviation from the observed data is high. The average tendency of simulated data can be measured using this technique. The optimal value of PBIAS is (0), and low values generally indicate accuracy in model simulation. When a positive value is obtained, it indicates underestimation bias, while a negative indicates overestimation bias (Moriasi et al., 2007). Along with the above-mentioned metrics, the RSR is another important statistical performance metric. It is the ratio of the RMSE and STDEV of measured data (Eq. 4), and a complementary indicator to the RMSE. The RSR varies from the optimal value of 0 to ∞, where zero indicates perfect model simulation, and a higher value represents lower model performance.

3.4 Model calibration and validation

High elevation variance remains a complex riddle in the SWAT modelling community. The WSRB has high heterogeneity in elevation with an altitudinal range of 610 to 7,019 m asl. Preliminary results show variations in the curve number from 36 to 92, indicating that modelling of the basin is perplexing. To overcome the model uncertainties incorporated with the physical structure of the SWAT model, 18 different modelling scenarios have been developed for this study, including DAs, HRUs, and EBs, while considering computational time as another dominating factor.

The WSRB is located in the Himalayan region of Nepal and this study could be beneficial for other similar Himalayan river basins. Three different values were used for the DA threshold: 25, 10, and 2.5K, with three different systems (10xSB, 5xSB, SB) for HRU generation. In the Himalayan region, the distribution of rainfall and temperature is not uniform, therefore, the addition of EBs to the model is crucial (Bhatta et al., 2019; Shrestha et al., 2017). Two different scenarios were considered—without EBs, and with EBs. The spatial variability of precipitation and temperature could be represented in the model by including EBs. The model allows for the consideration of lapse rates in temperature (TLAPS) and precipitation (PLAPS), in order to include elevation dependency. The model treats precipitation as either rainfall or snowfall, depending on air temperature with respect to the snowfall temperature, SFTMP (Shrestha et. al., 2017; Pradhanang et al., 2011).

Table 4 shows the calibration and validation results of different scenarios. Many researchers have suggested that the number of simulations for one iteration could be set between 500 and 1000. In this research, two iterations were performed—one with 500 model runs and another with 1000 model runs, to analyse the uncertainty effects from different numbers of DA thresholds, HRUs, and EBs. For both iterations and all model development scenarios, NSE was selected as an objective function with a value greater than 0.5. We carefully calibrated parameters such as Manning's constant for overland flow, Manning's constant for tributary channels, the average slope of tributary channels, and other hydraulic/geometric-related parameters by considering practical values. Detailed hydraulic modelling is needed to precisely estimate hydraulic parameters such as Manning's roughness coefficient (Ardiclioglu & Kuriqi, 2019). Since the focus of this study is on rainfall-runoff modelling rather than river analysis, no other hydraulic models are used.

4. Results and Discussions

4.1 Assessment of the SWAT model under different modelling scenarios

Table 4 shows the runtime for 1500 optimisation model runs in different modelling scenarios. The runtime for the model calibration is seen to be unaffected by EBs but varies considerably with the DA threshold and HRUs. It is obvious that a fewer number of SBs is generated by a higher DA threshold value and vice versa. The calibration runtime drastically increases with a rise in the number of SBs. In this study, three different SB population scenarios viz. 7, 27, and 73 showed that the runtime expeditiously increased from 0.74 to 19.43 hr. The model was simulated under three different HRU scenarios: 1) HRU = SB, 2) HRU = 5xSB, and 3) HRU = 10xSB. Under the 10xSB HRU scenario, the scenario with a large number of SBs produced better results but the runtime for model simulation was too high. From **Table 4** it is evident that an increase in the number of HRUs is highly sensitive to the runtime for model calibration. Surprisingly, an increase in the number of HRUs did not lead to a significant change in model performance.

Thus, a larger population of SBs and HRUs did not lead to longer runtimes in any of the EB scenarios without improving model performance. It is noteworthy that the modelling scenario for HRU = SB in the case of SB = 73 took only 1.51 hr. and HRU = 5xSB or 10xSB took 10.33 and 19.43 h, respectively but produced almost similar results. In the SWAT model, runoff from all HRUs within an SB are summed and enter the main reach of the SB before being routed through the channel network to the outlet of the watershed. The increase in the number of SBs significantly affects channel routing but the increase in the number of HRUs simply increases different hydrological responses inside the SB. If the geological, soil, and land use conditions are almost similar, then increasing the number of HRUs might go towards increasing the computational time rather than model performance. The selection of HRUs plays a pivotal role in replicating the unique hydrological response inside the SB. Consequently, we should be aware of the time required for model calibration, the number of HRUs and SBs and their impacts on model performance during the setup phase. This study provides some ideas on model development, runtime, and the impact of varying numbers of SBs and HRUs on model performance.

Next, we included EBs and conducted a second set of the previous nine scenarios. After adding the maximum EB, the model performance showed significant improvement when compared to the model without EB. This is attributed to the fact that the model (SWAT) attempts to capture the hydrology of the modelling domain using HRUs as its computational units. The assumption in SWAT is that the HRUs explain most of the variations in the basin's physical (and thus climatic) characteristics. However, in regions with large topographical gradients such as the

WSRB, the computational units (HRUs) themselves vary considerably in elevation. This results in high spatial temperature and precipitation variability which the HRUs, as individual units, are not able to simulate completely. Thus, each HRU itself requires further grouping based on elevation, which is exactly what the EB in SWAT does. With adequate representation of the lapse in temperature and precipitation with elevation, HRUs with EBs produce results concurring to reality via correct snow-rain distribution along the elevation. This greatly improves the overall water balance and hydrology representation of the model. Thus, in the Himalayan region (or any region with large topographical relief for that matter), the EB is very important for improving the SWAT model performance. This result is similar to that reported by Bhatta et al. (2019) for the eastern Himalayan region of Nepal.

Dhami et al. (2018) used the SWAT and snowmelt runoff model (SRM) in the Karnali River Basin. Their study reported that about 20% of precipitation falls as snowfall, 60% of which melts away, while more than 12% of river discharge is contributed by snowmelt runoff. Moderate Resolution Imaging Spectroradiometer (MODIS) snow cover products were used to derive the percentage of snow cover area in their study. A similar result was observed in another study (Shiwakoti, 2017) conducted in the Karnali River Basin using the HBV Light Model, where the contribution of snowmelt to annual flow was found to be about 11% with a maximum monthly contribution of almost 30% in May and a minimum of 2% in January. Shiwakoti (2017) reported a significant inter-annual variation in the snowmelt contribution. For instance, in the Seti River, snowmelt varied by up to a maximum of 27% in 1987 and a minimum of 11% in 1997.

These studies highlighted the spatio-temporal variability of snow accumulation and melt in the Himalayan watersheds. Currently, we limit our study of snowmelt and snow accumulation processes for a precise analysis, although simulated by considering EBs. We attempted to calibrate the parameters using a single site-based calibration of streamflow discharge. However, this study explores the spatio-temporal changes in snow cover areas developed by Muhammad & Thapa (2020). Snow, acting as water storage, is one of the crucial components of the hydrological cycle. The field measurement of a vast spatial extent of snow cover, especially in the Himalayan basin as in the study area, is quite a challenging task (Immerzeel et al., 2009). Therefore, the use of satellite-based information is common for assessing the snow extent. However, passive satellite remote sensing is constrained by persistent cloud. In order to minimise persistent cloud cover and obtain information under such conditions, eight-day composite snow cover products from MODIS were developed. Although the eight-day composite products reduced cloud cover, a significant amount of clouds remained which need to be removed. Muhammad & Thapa (2020) improved the MODIS onboard Terra and Aqua snow cover by employing different filters (seasonal, temporal, spatial, and different combinations) and validated using Landsat 8 for ground-truth. Their final product covers the period from mid-2002 to 2018 This study used the data from 2003 to 2009 to assess the association between snow cover changes and downstream streamflow (both observed and simulated).

Fig. 4 shows the model performance metrics and runtime to simulate 18 different scenarios conducted using the SWAT-CUP model and employing the SUFI-2 algorithm. Clearly, the performance metrics are better for scenarios in which EBs are included, compared to corresponding scenarios without EBs. Noticeably, the runtime did not differ significantly.

For hydrological prediction, great care is required to develop an acceptable model. Random generation of SB and HRUs will always lead to poor model performance with high levels of uncertainty. For good modelling practice, it is better to suggest the potential uncertainties associated with the number of SBs, HRUs, and EBs in the prediction of streamflow. In this study, different scenarios were calibrated using discharge data (1999 to 2005) and SUFI-2 at each station. Model structure and parameter uncertainties always exist, so fixing the number of SBs and HRUs is a great deal better for model calibration and achieving a better runtime. For further analysis in the subsequent section, the case with the highest number of SBs and HRUs is applied.

Fig.4

Table 4

4.2 Sensitivity analysis

The initial set of parameters considered (39 in total) for model calibration is shown in **Table 6**. This study employed the global sensitivity analysis method. The purpose of calibration is to adjust the value of the sensitive parameters so that the simulated flows match the observed. The graphical user interface details are available in the SWAT-CUP manual (Abbaspour, 2011). Sensitivity analysis was executed with 1500 model runs in two phases using the SWAT-CUP model. In the first phase, 500 model runs were made. Sensitive parameters were confirmed by looking at the p-value and t-stat. The parameters with the smallest p-value and the largest t-stat were considered as the most sensitive. The most sensitive parameters were (in decreasing order of sensitivity) LAT_TTIME.hru, CH_K2.rte, ALPHA_BNK.rte, and CN2.mgt. The new range for each parameter was once again adjusted and used for the next round of iterations (remaining 1000 model runs) and uncertainty analysis. The model parameters, including the final fitted value, new maximum and minimum values, t-stat, rank of sensitivity, p-values, together with an explanation of each are displayed in **Table 5**.

Table 5

4.3 Model performance during calibration and validation

To minimise the uncertainty in prediction, effort is required to parameterise the model for calibration and uncertainty analysis. The range of each parameter is crucial for calibrating the model for better agreement between observed and simulated values. The simulated and observed discharges were compared at the Gopaghat flow-gauging station (outlet) during calibration (1999 to 2005). The strength of calibration is shown by the shaded area in **Fig. 5**, as explained by r-factor. Upon close examination of the 95PPU band, the prediction bandwidth was considered to be very high (especially for peak discharges), indicating significant uncertainty. The p-factor and r-factor values obtained during calibration were 0.82 and 0.80, respectively. Similarly, the values for R^2, NSE, RSR, and PBIAS were observed as 0.84, 0.82, 0.42, and 10.5, respectively during calibration, representing better performance for simulation than observed.

Validation establishes the strength of the calibrated model for practical applications and if the objective functions are not achieved for the validation dataset, the calibration and/or model assumptions will need to be revisited. The observed and simulated flow, including precipitation patterns are plotted in **Fig. 6** during calibration and validation, showing good agreement during low and high flows. Moriasi et al. (2007) suggested the general performance of objective functions. **Fig. 7** shows the relationship between observed and simulated variables with good correlation ($R^2 = 0.84$) for both calibration and validation phases. A closer look into the temporal variation of river discharge (**Fig. 6**) and scatter plots (**Fig. 7**) indicates that the model effectively captured both low flow and high flow in an agreeable manner. Some of the observed high flows were not effectively captured by the model. The model performance during calibration and validation is presented in **Table 6**. The p-factor, r-factor, R^2, NSE, RSR, and PBIAS values during validation were 0.79, 0.72, 0.84, 0.83, 0.42, and 12.6, respectively. Overall, the model was found to be appropriate for water resource assessment. Importantly, if the model is to be used for extreme flow analysis such as flood forecasting then careful calibration remains necessary, focusing on the precise simulation of peak flow. In addition, a daily simulation time step and continuous time marching, limit the application of SWAT for detailed, event-based flood simulation.

Fig. 5

Fig. 6

Fig. 7

Table 6

4.4 Snow cover and its association with streamflow

Fig. 8 shows the spatial distributions of snow cover across the study area for different months with ≥20 (up to 24) MODIS eight-day composite images available for different months in the period from 2003–2008. The occurrences of snow in each MODIS eight-day composite image were normalised by the number of composite images in that month, expressed in percentage terms. The areas with 100% values indicate the extent of monthly snow cover in the study area. From the beginning of May, the snow cover starts to decrease, indicating the significant contribution of snowmelt. During the monsoon season (Jun–Sep), the extent of snow cover is limited to only high altitudes. On a monthly scale, the mean monthly snow cover area is found to be the highest (~1700 km^2) in February followed by March, with June the lowest (~650 km^2) followed by August. A temporal intra-annual fluctuation of almost 1000 km^2 significantly influences the downstream streamflow. The inter-annual variation shows that 2005 exhibited the highest extent of snow cover (~1200 km^2), with adjacent years 2004 and 2006 having the lowest (~1000 km^2) across the study area during the analysis period from 2003–2008. Highly dynamic intra- and inter-annual variations in snow cover are integral characteristics of the study area. Hydrological monitoring stations at immediate outlets of snow-covered sub-catchments are necessary for a detailed analysis of snow accumulation and melting mechanisms, and their effect on streamflow.

Fig. 9 shows the temporal variations in the eight-day snow cover area (data available in the supplemental section), basin-averaged daily temperature (average, maximum and minimum), and mean daily discharge (both observed and simulated) at the Gopaghat hydrological monitoring station, which is far downstream of snow-fed SBs. Though a clear association is difficult to find between temporal changes in the extent of snow cover and streamflow due to the larger proximity, a general indication of a greater snowmelt contribution is shown during the late pre-monsoon time (around May). Almost 90% of annual precipitation occurs in the period from May to October and only about 10% in the remaining six months. Due to an increase in temperature from May, precipitation normally occurs in the form of liquid (i.e. rainfall) except in high land (> 5000 m asl). Precipitation during late post-monsoon and winter contributes as snow accumulation, and increased snow cover (**Figs 8-9**) also demonstrated the same mechanism. From the start of April, the snow cover slowly begins to reduce with the rate peaking by May with an increase in temperature. Normally, precipitation also noticeably increases from April, becoming even more noticeable by the end of May before the onset of monsoon around June.

4.5 Projection of precipitation, temperature, and discharge

Fig. 10 shows the inter-annual variations of the projected annual precipitation from 2020 to 2099 under two warming scenarios with fluctuating deviations. There was no clear difference in the tendency of annual precipitation to fluctuate under the two warming scenarios. However, a clear indication of the incremental frequency of extreme precipitation (both drier and wetter events) was depicted by all selected climate models. The RCPs represent the range of greenhouse gas (GHG like CH_4, CO_2, N_20, and $S0_2$) emissions which have a clear proportional relationship with temperature. Changes in precipitation for a warming world will not be uniform. The MME of selected climate models showed a slightly increasing trend of annual precipitation, with monsoon precipitation likely to intensify. The rate of increase was slightly higher for the RCP 8.5 scenario. Time-sliced average analyses were conducted for three time periods (F1, F2, and F3) under two warming scenarios (RCPs 4.5 and 8.5). The deviations of mean annual precipitation with respect to the baseline for different cases are shown in **Fig. 11**, derived from individual climate models and the MME of selected climate models.

Fig. 10

Fig. 11

Except for ACCESS1-0, all selected climate models showed an increasing trend for mean annual precipitation in different future scenarios. The GFDL-CM3 showed a moderate increasing trend whereas CNRM-CM5 and MPI-ESM-LR showed larger increasing trends. According to the MME of four selected climate models, the mean annual precipitation could increase by 9.65% (9.66) during the F1 time period, 10.45% (10.53) during the F2 time period, and 6.94% (7.64) during the F3 time period under RCP 4.5 (RCP 8.5) with respect to the baseline. The F2 time period was found to be the wettest among the three selected time periods (F1, F2, and F3).

Fig. 12 shows the inter-annual variations of the projected annual T_{avg} from 2020 to 2099 under two warming scenarios. Unlike precipitation, the projection showed a clear rising trend in the annual T_{avg}. This is a similar result to that reported by Pandey et. al (2019) in the Chamelia watershed—a tributary of Mahakali. Mahakali is an adjacent watershed located to the west of the WSRB. As expected, the rate of increase in the T_{avg} was higher under RCP 8.5 than RCP 4.5. Time-sliced average deviations with respect to the baseline were conducted for the six different cases mentioned above (shown in **Fig. 13)**, derived from individual climate models and the MME of selected climate models. All selected climate models clearly indicated rises in temperature. The MME of the six selected climate models showed that the mean annual T_{avg} could increase by 0.76 °C (varying from 0.44 to 1.45) during the F1 time period, 1.14 °C (varying from 0.92 to 1.5) during the F2 time period, and 1.55 °C (varying from 1.2 to 2.17) during the F3 time period under RCP 4.5 with respect to the baseline. The ACCESS1-0 showed the projected highest mean annual T_{avg} for F2 and F3 time periods, and CCSM4 for the F1 time period under RCP 4.5. The CNRM-CM5 projected the lowest mean annual T_{avg} for F1 and F2 time periods, and CCSM4 for the F3 time period under RCP 4.5.

Under RCP 8.5, the MME showed that the mean annual T_{avg} could increase by 0.92 °C (varying from 0.57 to 1.33) during the F1 time period, 2.11 °C (varying from 1.55 to 3.24) during the F2 time period, and 3.9 °C (varying from 3.06 to 5.34) during the F3 time period with respect to the baseline. The GFDL-CM3 showed the highest mean annual T_{avg} for all three time periods under RCP 8.5. In similarity to the warming scenario RCP 4.5, CNRM-CM5 provided the projected lowest mean annual T_{avg} for F1 and F2 time periods, and CCSM4 for the F3 time period under RCP 8.5.

Fig. 12

Fig. 13

Fig. 14 shows the mean monthly precipitation and temperature (T_{max}, T_{min}, and T_{avg}) for the baseline (dashed) and different projected scenarios. The patterns of precipitation and temperature were almost congruous with the baseline. In the case of temperature, a linear upward shift, meaning an anticipated rising temperature, was visible for all future scenarios. The increments were higher under RCP 8.5 than RCP 4.5, and could continue with the evolution of time. During the F1 time period, the mean annual T_{max} (T_{min}) could increase by 0.81 °C (0.71) under RCP 4.5 and 0.9 °C (0.94) under RCP 8.5 with respect to the baseline. During the F2 time period, the mean annual T_{max} (T_{min}) could increase by 1.05 °C (1.23) under RCP 4.5 and 2.01 °C (2.22) under RCP 8.5 with respect to the baseline. Similarly, During the F3 time period, the mean annual T_{max} (T_{min}) could increase by 1.44 °C (1.66) under RCP 4.5 and 3.72 °C (4.09) under RCP 8.5 with respect to the baseline. The rate of increase was higher for T_{min} than T_{max} except in the case of RCP 4.5 F1. The MME showed that the deviation in mean monthly T_{avg} could be highest in November, i.e. +5.0 °C (varying from +4.1 to +6.2), and the lowest in June, i.e. +2.7 °C (varying from +1.6 to +4.2) in the F3 time period under RCP 8.5 with respect to the baseline. In general, the rate of increase in temperature was found to be higher from October to February. Therefore, the WSRB is expected to see comparatively warmer winters in the coming decades.

In the case of precipitation, various climate models showed different projections (larger spreads including both positive and negative deviations with respect to the baseline can be found in **Fig. 14**). The MME of selected climate models showed a slight increasing deviation with respect to the baseline in the coming days. On a monthly scale, both positive and negative deviations with respect to the baseline were found for different future scenarios.

Fig. 14

Noticeably, the highest rainfall month could shift from July to August for the baseline time period, with a greater chance of increasing precipitation during Jan–Mar and Oct–Nov in the coming days than the baseline condition. On a seasonal scale, the deviation with respect to the baseline could be +14.7% (from -48.7 to +114.1) for the winter (DJF), +50.2% (from -12.2 to +136.6) for the pre-monsoon (MAM), -2.5% (from -21.8 to +22.3) for the monsoon (JJAS), and +124.8% (from +95.1 to +155.5) for the post-monsoon (ON) under RCP 4.5 during the F3 time period. Similarly, under RCP 8.5, the deviation with respect to the baseline could be -12.6% (from -56.0 to +43.3) for the winter, +68.1% (from +8.5 to +123.3) for the pre-monsoon, -2.4% (from -16.8 to +14.7) for the monsoon, and +152.9% (from +126.6 to +174.6) for the post-monsoon under RCP 8.5. The combination of projected changes in precipitation and temperature would significantly affect the water balance. The likely impacts on water scarcity and river floods mandate proper water resources management under changing climate.

Fig. 15

Fig. 15 shows the mean monthly river discharge of the baseline (dashed) and different projected scenarios. In general, wet seasons would be even wetter and dry seasons even drier in the coming days. According to the MME, on a monthly scale, the mean monthly river discharge could deviate by +24.8% (-9.2) in Jan, +88.4% (+76.2) in Feb, +69.7% (+87.7) in Mar, +44.7% (+66.5) in Apr, +45.7% (+54.6) in May, +68.7% (+75.6) in Jun, +20.6% (+25.9) in Jul, +2.5% (+7.6) in Aug, -5.0% (+6.3) in Sep, -28.2% (-22.6) in Oct, -53.2% (-51.8) in Nov, and -59.5% (-59.7) in Dec with respect to the baseline in the F3 time period under RCP 4.5 (RCP 8.5). Lower percentage deviations were observed for the months of August and September. However, one important factor needs to be addressed, namely that the river flow during the monsoon season is very high and a +10% increment in mean monthly discharge indicates a higher absolute value for river discharge. In addition, the large ranges displayed by different climate models (coloured blue in **Fig. 15**) represent higher uncertainties, depending on climate model selection. Anticipated changes in monthly river discharge can significantly impact on water consumption planning. For instance, a decrease in the available discharge during the winter season will increase pressure on the water supply, irrigation, and hydropower plants. While an increase in discharge during the monsoon season will not provide any significance for water resources projects because the flow above the design discharge is generally spilled out.

Fig. 16

Fig. 16 a–b shows the flow duration curves of mean daily discharge for the baseline and three different future time periods under two warming scenarios. A clear upward shift could be seen in time flow, equal to or exceeding 10 to 35%, in the coming days in all future scenarios. Under RCP 4.5, Q_{10} = 507 m^3/s in the baseline time period could increase to about 590 m^3/s during F1 and F2 time periods and about 560 m^3/s during the F3 time period. While Q_{20} = 326 m^3/s in the baseline time period could increase to about 450 m^3/s during F1 and F2 time periods and about 425 m^3/s during the F3 time period under RCP 4.5. Similarly, Q_{30} = 202 m^3/s in the baseline time period could increase to about 290 m^3/s during F1 and F3 time periods and about 300 m^3/s during the F2 time period under RCP 4.5. A similar tendency was observed under RCP 8.5. Water resources projects are expected to depend significantly on the length of time the available flow is around 20–30% (for instance, runoff, river type, and hydropower) and could get increased river discharge. There are seven licensed hydropower projects across the study area (**Fig. 16 c–d**) with a capacity of >500 MW and a few proposed hydropower projects, including one >750 MW (not shown). These projects are likely to be significantly affected under changing climate.

At the same time, the length of time the available flow is equal to or more than 80% (low or base flow) may reduce under the future projection which might have a negative impact on water resource projects depending on perennial long-term low flows such as water supply, irrigation, agriculture, aquaculture, and other environmental/aquatic systems. A better understanding of the anticipated change in the timing of streamflow (low, medium, and high) and trends under changing climate is necessary for effective water resources management (Dinpashoh et al., 2019).

Fig. 17

Fig. 17 shows the mean annual river discharge of the baseline and various projected scenarios using different climate models. According to the climate models, the mean annual river discharge could decrease for ACCESS1-0 under RCP 4.5 in the F3 time period with respect to the baseline. Different climate models exhibited variations in the level of river discharge. The CNRM-CM5 and MPI-ESM-LR showed a greater increase, ACCESS1-0 a lesser increase, and GFDL-CM3 a moderate increase in river discharge in the coming days with respect to the baseline. The MME showed that a larger discharge could occur in the F2 time period compared to the F1 and F3. Under RCP 4.5, the mean annual river discharge would increase by 15.2% in the F1 time period, 17.3% in the F2 and 12.5% in F3 with respect to the baseline. Similarly, under RCP 8.5, the mean annual river discharge would increase by 16.4% in the F1 time period, 19.9% in F2, and 18.3% in F3 with respect to the baseline. Overall, increased streamflow is projected in the coming days. The planning of future water resources projects may benefit from this information.

Fig. 18

Fig. 18 shows the mean seasonal river discharge for the MME of the baseline and different future scenarios. We found that the mean seasonal river discharge could decrease during the post- monsoon for all scenarios, and during winter under RCP 8.5 in F3 with respect to the baseline. The MME showed an increasing pattern of mean seasonal river discharge for pre-monsoon. Under RCP 4.5, the pre-monsoon river discharge could increase by 11.9% in the F1 time period, 30.0% in F2, and 50.6% in F3 with respect to the baseline. Similarly, under RCP 8.5, pre-monsoon river discharge could increase by 12.4% in the F1 time period, 37.5% in F2, and 65.5% in F3 with respect to the baseline. In contrast, post-monsoon river discharge would continuously decrease in the coming days. The monsoon river discharge is more likely to increase to the maximum during the F2 time period than in the F1 and F3. The projected change in winter river discharge is comparatively low.

In the future, there may be various water resources projects (small to large scale) in the study area. Our study suggests that changing streamflow should be considered during the planning process. The results of this study may provide a benchmark for water availability in the basin. With potential hydropower development across the study area, water balance quantification is crucial. Our future work would include calibrating water balance components such as the soil moisture content and quantifying the anticipated impacts of changing climate on individual water balance components (infiltration, subsurface flow, soil moisture content, percolation, and others).

5. Conclusions

The first objective of this study was to analyse model uncertainty resulting from various modelling scenarios i.e. the number of SBs, HRUs, and EBs. The model SUFI-2 in SWAT-CUP was applied for calibration/uncertainty analysis, validation, and sensitivity analysis. To simulate daily streamflow, the SWAT model was calibrated and validated for 18 different modelling scenarios using the SUFI-2 algorithm. The SWAT hydrological model was applied to a mountainous watershed in Western Nepal (WSRB). First, 18 different modelling scenarios were developed to analyse model uncertainty in daily simulations.

The performance of different scenarios was compared through evaluating the p-factor, r-factor, R^2, NSE, and PBIAS to achieve the best simulation. Model calibration performance and parameter sensitivity were evaluated using four objective functions (R^2, NSE, PBAIS, and RSR) applying SUFI-2. The p-factor, r-factor, R^2, NSE, PBIAS, and RSR values during calibration were 0.82, 0.80, 0.84, 0.82, 7.2, and 0.42, respectively, and 0.79, 0.72, 0.83, 0.82, 11.8, and 0.42, respectively during validation. The results indicate that the parameters LAT_TTIME, CH_K2, ALPHA_BNK, CN2, PLAPS, and TLAPS were the most sensitive and significantly impacted the streamflow simulations in Himalayan catchments. The SUFI-2 algorithm was successfully employed to calibrate and validate the daily streamflow of SWAT in the mountainous region. It can be concluded that the inclusion of EBs during the SWAT model setup is of paramount importance for high mountain basins, improving model performance without compromising runtime. By applying the results of this study, we believe that hydrologists and other stakeholders can quickly evaluate various management scenarios and make effective and optimum decisions.

As part of the second objective, we applied the model to assess the anticipated river discharge under the changing climate. We used four RCMs for precipitation, six RCMs for temperature, and their MMEs under two RCPs for projected analysis. Three future time periods (F1, F2, and F3) were analysed. The CNRM-CM5 and MPI-ESM-LR showed greater increases, ACCESS1-0 showed a lesser increase and GFDL-CM3 showed a moderate increase in river discharge for the coming days with respect to the baseline. The MME showed that a larger discharge could occur in the F2 time period compared to the F1 and F3. Under RCP 8.5, the mean annual river discharge could increase by 16.4% in the F1 time period, 19.9% in F2, and 18.3% in F3 with respect to the baseline. Notably, pre-monsoon river discharge could increase by 12.4% in the F1 time period, 37.5% in F2, and 65.5% in F3 with respect to the baseline under RCP 8.5. In general, our results show that precipitation could increase slightly (higher during the F2 time period), with the temperature rising significantly (continuous rising trend), and the river discharge moderately increasing (higher during the F2 period).

This study provides a rigorous analysis of the computational aspect of hydrological modelling together with useful insight for practitioners involved in the operation of the SWAT for which model runtime is critical. In addition, the case study under focus here has been conducted in one of the top four most vulnerable basins to climate change in Nepal and the area also includes a major storage-type hydropower project. Our conclusions regarding the anticipated shift of the flow duration curve in the case study will be helpful to various stakeholders such as hydropower/water resource planners for effective water resource management. The results of this paper thus have additional contemporary significance which will definitely benefit decision-making in scientific circles.

Acknowledgement

The research team would like to express their thanks to the DHM, Nepal for providing the required dataset for this study. We are also grateful to the Water Engineering and Management (WEM) department of the Asian Institute of Technology (AIT) for providing a high-speed computer for model calibration and validation. Our sincere thanks also go to Amrit Thapa for his help in accessing data on snow cover and the anonymous reviewers for their constructive comments and suggestions.

References

Abbaspour, K. C., Yang, J., Maximov, I., Siber, R., Bogner, K., Mieleitner, J., … Srinivasan, R. (2007). Modelling hydrology and water quality in the pre-alpine/alpine Thur watershed using SWAT. Journal of Hydrology, 333(2–4), 413–430. doi:10.1016/j.jhydrol.2006.09.014

Abbaspour, K. (2007). User manual for SWAT-CUP, SWAT calibration and uncertainty analysis programs. *Swiss Federal Institute of Aquatic Science and Technology, Eawag, Duebendorf, Switzerland*.

Abbaspour, K. (2011). User Manual for SWAT-CUP: SWAT Calibration and Uncertainty Analysis Programs. Eawag: Swiss Fed. Inst. of Aquat. *Sci. and Technol., Duebendorf, Switzerland*, 103.

Abbaspour, K. C., Rouholahnejad, E., Vaghefi, S., Srinivasan, R., Yang, H., & Kløve, B. (2015). A continental-scale hydrology and water quality model for Europe: Calibration and uncertainty of a high-resolution large-scale SWAT model. *Journal of Hydrology, 524*, 733–752.

Agarwal, A., Babel, M. S., & Maskey, S. (2015) Estimating the impacts and uncertainty of climate change on the hydrology and water resources of the Koshi River Basin. In: Shrestha, S., Anal, A., Salam, P., & van der Valk, M. (eds) Managing water resources under climate uncertainty: Examples from Asia, Europe, Latin America, and Australia. Springer Water. Springer. 105-126. doi: https://doi.org/10.1007/978-3-319-10467-6_6

Alcamo, J., Doll, P., Henrichs, T., Kaspar, F., Lehner, B., Rosch, T., & Siebert, S. (2003) Global estimates of water withdrawals and availability under current and future "business-as-usual" conditions. *Hydrological Sciences Journal*, 48:339–348.

Alcamo, J., Florke, M., & Marker, M. (2007) Future long-term changes in global water resources driven by socioeconomic and climatic changes. *Hydrological Sciences Journal*, 52, 247–275.

Ardıçlıoğlu, M.; Kuriqi, A. Calibration of channel roughness in intermittent rivers using HEC-RAS model: Case of Sarimsakli Creek, Turkey. SN Appl. Sci. 2019, 1

Arnold, J. G., Moriasi, D. N., Gassman, P. W., Abbaspour, K. C., White, M. J., Srinivasan, R., . . . Van Liew, M. W. (2012). SWAT: Model use, calibration, and validation. *Transactions of the ASABE, 55*(4), 1491–1508.

Aryal, A., Shrestha, S., & Babel, M. S. (2018). Quantifying the sources of uncertainty in an ensemble of hydrological climate-impact projections. *Theoretical and Applied Climatology*, 1–17 2359–3.

Azmat, M., Qamar, M. U., Huggel, C., & Hussain, E. (2018). Future climate and cryosphere impacts on the hydrology of a scarcely gauged catchment on the Jhelum river basin, Northern Pakistan. Science of the Total Environment, 639, 961–976. https://doi.org/10.1016/j.scitotenv.2018.05.206

Bajracharya, A. R., Bajracharya, S. R., Shrestha, A. B., & Maharjan, S. B. (2018). Climate change impact assessment on the hydrological regime of the Kaligandaki Basin, Nepal. *Science of the Total Environment, 625*, 837–848.

Bhatta, B., Shrestha, S., Shrestha, P. K., & Talchabhadel, R. (2019) Evaluation and application of a SWAT model to assess the climate change impact on the hydrology of the Himalayan River Basin. *Catena* 181: 104082.

Chaibou Begou, J., Jomaa, S., Benabdallah, S., Bazie, P., Afouda, A., & Rode, M. (2016). Multi-site validation of the SWAT model on the Bani catchment: model performance and predictive uncertainty. *Water, 8*(5), 178.

Chaulagain, N. P. (2006) Impacts of Climate Change on Water Resources of Nepal: The Physical and Socioeconomic Dimensions. *Ph.D Thesis*, University of Flensburg.

Clark, M. P., Rupp, D. E., Woods, R. A., Zheng, X., Ibbitt, R. P., Slater, A. G., . . . Uddstrom, M. J. (2008). Hydrological data assimilation with the ensemble Kalman filter: Use of streamflow observations to update states in a distributed hydrological model. *Advances in Water Resources, 31*(10), 1309–1324.

Croton, D. J., Stevens, A. R., Tonini, C., Garel, T., Bernyk, M., Bibiano, A., . . . Shattow, G. M. (2016). Semi-analytic galaxy evolution (sage): Model calibration and basic results. *The Astrophysical Journal Supplement Series, 222*(2), 22.

Dahal, V., Shakya, N. M., & Bhattarai, R. (2016). Estimating the impact of climate change on water availability in Bagmati basin, Nepal. *Enviromental Processes*, 3(1), 1–17. doi: https://doi.org/10.1007/s40710-016-0127-5.Dinpashoh, Y., Singh, V. P., Biazar, S. M. & Kavehkar, S. (2019). Impact of climate change on streamflow timing (case study: Guilan Province). *Theoretical and Applied Climatology*, 138, 65–76. doi: https://doi.org/10.1007/s00704-019-02810-2.

Dhami, B., Himanshu, S. K., Pandey, A., & Gautam, A. K. (2018). Evaluation of the SWAT model for water balance study of a mountainous snowfed river basin of Nepal. Environmental Earth Sciences, 77(1), 1–20. https://doi.org/10.1007/s12665-017-7210-8

Gassman, P. W., M. Reyes, C. H. Green, & J. G. Arnold. (2007). The Soil and Water Assessment Tool: Historical development, applications, and future directions. *Transactions of the ASABE* 50(4): 1211–1250.

Gassman, P. W., & Yingkuan, W. (2015). IJABE SWAT Special Issue: Innovative modeling solutions for water resource problems. *International Journal of Agricultural and Biological Engineering, 8*(3), 1–8.

Gautam, S., Dahal, V. & Bhattarai, R. (2019). Impacts of DEM source, resolution and area threshold values on SWAT generated stream network and streamflow in two distinct Nepalese catchments. Environmental Processes, 1–21. doi: https://doi.org/10.1007/s40710-019-00379-6

Gurung, P., Bharati, L., & Karki, S. (2013). Application of the SWAT Model to assess climate change impacts on water balances and crop yields in the West Seti River Basin. *Proceedings of the 2013 International SWAT Conference*, Toulouse, France, 17–19 July 2013, 175–191.

Gladfelter, S. (2018). The politics of participation in community-based early warning systems: Building resilience or precarity through local roles in disseminating disaster information? *International Journal of Disaster Risk Reduction, 30*, 120–131.

Gurung, P., Bharati, L., & Karki, S. (2015). Impact of climate change and watershed interventions on water balance and crop yield in West Seti River sub-basin of Nepal. *Journal of Hill Agriculture, 6*(2), 219–227.

Hagemann, S., Chen, C., Clark, D. B., Folwell, S., Gosling, S. N., Haddeland, I., Hanasaki, N., Heinke, J., Ludwig, F., Voss, F., & Wiltshire, A. J. (2013). Climate change impact on available water resources obtained using multiple global climate and hydrology models. *Earth System Dynamics*, 4, 129–144, doi: 10.5194/esd-
4-129-2013.

Hanasaki, N., Fujimori, S., Yamamoto, T.,Yoshikawa, S., Masaki, Y., Hijioka, Y., Kainuma, M., Kanamori Y., Masui, T., Takahashi, K., & Kanae, S. (2013). A global water scarcity assessment under Shared Socio-economic Pathways – Part 2: water availability and scarcity. *Hydrology and Earth System Sciences*, 17, 2393–2413.

Hirabayashi, Y., Kanae, S., Emori, S., Oki, T., & Kimoto, M. (2008) Global projections of changing risks of floods and droughts in a changing climate. *Hydrological Sciences Journal*, 53, 754–772.

Hirabayashi,Y., Mahendran, R., Koirala, S., Konoshima, L., Yamazaki, D., Watanabe, S., Kim, H., & Kanae, S. (2013) Global flood risk under climate change. *Nature Climate Change*, 3, 816–821. doi: 10.1038/ nclimate1911

Immerzeel, W. W., Droogers, P., De Jong, S. M., Bierkens, M. F. P. (2009). Large-scale monitoring of snow cover and runoff simulation in Himalayan river basins using remote sensing, Remote Sens. Environ., 113(1), 40–49, doi:10.1016/J.RSE.2008.08.010.

Immerzeel, W. W., van Beek, L. P. H., & Bierkens, M. F. P. (2010). Climate change will affect the Asian water towers. *Science* 328 (5984), 1382–1385.

Immerzeel, W. W., Pellicciotti, F., & Bierkens, M. F. P. (2013). Rising river flows throughout the twenty-first century in two Himalayan glacierized watersheds. *Nature Geoscience*, 6, 742–745.

Karki, R., Talchabhadel, R., Aalto, J., & Baidya S. K. (2016). New climatic classification of Nepal. Theoretical and Applied Climatology, 125 (3–4), 799–808.

Karki, S. (2012). Application of uncertainty analysis techniques to SWAT model: a case study of West Seti River basin, Nepal. *MSc Thesis*. Department of Civil Engineering, Institute of Engineering, Pulchowk Campus, Tribhuvan University, Nepal.

Khadka, D., Babel, M. S., Shrestha, S., & Tripathi, N. K. (2014). Climate change impact on glacier and snow melt and runoff in Tamakoshi basin in the Hindu Kush Himalayan (HKH) region. *Journal of Hydrology, 511*, 49–60.

Krause, P., Boyle, D. P. & Base, F. (2005). Comparison of different efficiency criteria for hydrological model assessment. *Advances in Geosciences* 5: 89–97.

Krysanova, V., & White, M. (2015). Advances in water resources assessment with SWAT—an overview. *Hydrological sciences journal, 60*(5), 771–783.

Lenderink, G., Buishand, A., & Deursen, W. V. (2007). Estimates of future discharges of the river Rhine using two scenario methodologies: direct versus delta approach. *Hydrology and Earth System Sciences, 11*(3), 1145–1159.

Liu, W., Dugar, S., McCallum, I., Thapa, G., See, L., Khadka, P., . . . Shakya, P. (2018). Integrated Participatory and Collaborative Risk Mapping for Enhancing Disaster Resilience. *Isprs International Journal of Geo-Information, 7*(2).

Maharjan, L. D. (2012). Nepal: Building Climate Resilience in Watersheds in Mountain Eco-Regions.

McSweeney, C. F., Jones, R. G., Lee, R. W., & Rowell, D. P. (2015). Selecting CMIP5 GCMs for downscaling over multiple regions, *Climate Dynamics*, 44, 3237–3260.

Mishra, Y., Nakamura, T., Babel, M. S., Ninsawat, S., & Ochi, S. (2018). Impact of climate change on water resources of the Bheri River Basin, Nepal. *Water*, 10(2): 1–21.

Moriasi, D. N., Arnold, J. G., Van Liew, M. W., Bingner, R. L., Harmel, R. D., & Veith, T. L. (2007). Model evaluation guidelines for systematic quantification of accuracy in watershed simulations. *Transactions of the Asabe, 50*(3), 885–900.

Muhammad S, Thapa A. (2020). An improved Terra-Aqua MODIS snow cover and Randolph Glacier Inventory 6.0 combined product (MOYDGL06*) for high-mountain Asia between 2002 and 2018. Earth System Science Data, 12(1): 345–356. https://doi.org/10.5194/essd-12-345-2020.

Nepal, S. (2016) Impacts of climate change on the hydrological regime of the Koshi river basin in the Himalayan region. Journal of Hydro-Environment Research 10: 76–89.

Pandey, V. P., Dhaubanjar, S., Bharati, L., & Thapa, B. R. (2019) Hydrological response of Chamelia watershed in Mahakali Basin to climate change. *Science of the Total Environment* 650: 365–383.

Piman, T., Cochrane, T. A., Arias, M. E., Dat, N. D., & Vonnarart, O. (2015) Managing Hydropower Under Climate Change in the Mekong Tributaries. In: Shrestha, S., Anal, A., Salam, P., & van der Valk, M. (eds) Managing water resources under climate uncertainty: Examples from Asia, Europe, Latin America, and Australia. Springer Water. Springer. 105–126. doi: https://doi.org/10.1007/978-3-319-10467-6_11

Portoghese, I., Vurro, M., & Lopez, A. (2015) Assessing the Impacts of Climate Change on Water Resources: Experiences from the Mediterranean Region. In: Shrestha, S., Anal, A., Salam, P., & van der Valk, M. (eds) Managing water resources under climate uncertainty: Examples from Asia, Europe, Latin America, and Australia. Springer Water. Springer. 105–126. doi: https://doi.org/10.1007/978-3-319-10467-6_9

Pradhan, P., Tingsanchali, T., Shrestha, S. (2019). Evaluation of Soil and Water Assessment Tool and Artificial Neural Network Models for hydrologic simulation in different climatic regions of Asia. *Science of the Total Environment* 701: 134308.

Pradhanang, S. M., Anandhi, A., Mukundan, R., Zion, M. S., Pierson, D. C., Schneiderman, E. M., Matonse, A., & Frei, A. (2011). Application of SWAT model to assess snowpack development and streamflow in the Cannonsville watershed, New York, USA. Hydrological Processes, 25(21), 3268–3277. https://doi.org/10.1002/hyp.8171

Refsgaard, J. C. (1997). Parameterisation, calibration and validation of distributed hydrological models. *Journal of Hydrology, 198*(1-4), 69–97.

Setegn, S. G., Srinivasan, R., Melesse, A. M., & Dargahi, B. (2010). SWAT model application and prediction uncertainty analysis in the Lake Tana Basin, Ethiopia. *Hydrological Processes: An International Journal, 24*(3), 357–367.

Shen, Z., Chen, L., & Chen, T. (2012). Analysis of parameter uncertainty in hydrological and sediment modeling using GLUE method: a case study of SWAT model applied to Three Gorges Reservoir Region, China. *Hydrology and Earth System Sciences, 16*(1), 121–132.

Shiwakoti, S. (2017). Hydrological Modeling and Climate Change Impact Assessment Using HBV Light Model: A Case Study of Karnali River Basin. XVI World Water Congress, 1–19.

Shrestha, M., Acharya, S. C., & Shrestha, P. K. (2017). Bias correction of climate models for hydrological modelling—are simple methods still useful? *Meteorological Applications*, 24, 531–539.

Shrestha, N. K., Du, X., & Wang, J. (2017). Assessing climate change impacts on fresh water resources of the Athabasca River Basin, Canada. Science of the Total Environment, 601–602, 425–440. https://doi.org/10.1016/j.scitotenv.2017.05.013

Shrestha, S., Bhatta, B., Shrestha, M., & Shrestha, P. K. (2018). Integrated assessment of the climate and landuse change impact on hydrology and water quality in the Songkhram River Basin, Thailand. *Science of the Total Environment, 643*, 1610–1622.

Shrestha, N. K., & Wang, J. (2018). Predicting sediment yield and transport dynamics of a cold climate region watershed in changing climate. Science of the Total Environment, 625, 1030–1045. https://doi.org/10.1016/j.scitotenv.2017.12.347

Singh, P., & Bengtsson, L. (2004). Hydrological sensitiviy of a large Himalayan basin to climate change, *Hydrological Processes*, 18, 2363–2385.

Smith, P. J., Brown, S., & Dugar, S. (2017). Community-based early warning systems for flood risk mitigation in Nepal. *Natural Hazards and Earth System Sciences, 17*(3), 423–437.

Talchabhadel, R., Karki, R., Thapa, B. R., Maharjan, M., & Parajuli, B. (2018). Spatio-temporal variability of extreme precipitation in Nepal. International Journal of Climatology, 38(11), 4296–4313. https://doi.org/10.1002/joc.5669

Talchabhadel, R., & Karki, R. (2019). Assessing climate boundary shifting under climate change scenarios across Nepal. *Environmental Monitoring and Assessment*, 191, 520. doi: https://doi.org/10.1007/s10661-019-7644-4

Tong, S. T. Y., & Chen, W. L. (2002). Modeling the relationship between land use and surface water quality. *Journal of Environmental Management, 66*(4), 377–393. doi: 10.1006/jema.2002.0593

Yang, J., Reichert, P., Abbaspour, K. C., Xia, J., & Yang, H. (2008). Comparing uncertainty analysis techniques for a SWAT application to the Chaohe Basin in China. *Journal of Hydrology, 358*(1–2), 1–23.

Zhang, D., Chen, X., Yao, H., & Lin, B. (2015). Improved calibration scheme of SWAT by separating wet and dry seasons. *Ecological Modelling, 301*, 54–61. doi: https://doi.org/10.1016/j.ecolmodel.2015.01.018

Table 1 Description of land use/ land cover and soil types

SN	SWAT class	Description	Area (km^2)	Area (%)
Land use types				
1	FRST	Forest mixed	1725.34	39.74
2	RNGB	Range-brush	192.18	4.43
3	PAST	Pasture (Grassland)	887.24	20.43
4	AGRL	Agricultural land	736.10	16.95
5	BARR	Barren	622.08	14.33
6	WATR	Water body	13.42	0.31
7	SNGL	Snow/glacier	165.65	3.82
8	URBN	Residential	0.09	0.00
Soil types				
1		GLACIER	28.39	0.65
2		Gleyic CAMBISOLS	6.38	0.15
3		Chromic CAMBISOLS	215.27	4.96
4		Eutric CAMBISOLS	983.24	22.65
5		Dystric REGOSOLS	1002.52	23.09
6		Humic CAMBISOLS	562.33	12.95
7		Eutric REGOSOLS	58.13	1.34
8		Gelic LEPTOSOLS	1485.70	34.22

Table 2 List of meteorological and hydrological stations in study area

Station Number	Name of Station	Data Type	Data frequency
104	Dadeldhura	(Prcp, Temp)	Daily (1996 - 2008)
201	Pipalkot	(Prcp)	Daily (1996 - 2008)
202	Chainpur (west)	(Prcp, Temp)	Daily (1996 - 2008)
211	Khaptad	(Prcp)	Daily (1996 - 2008)
218	Dipayal (doti)	(Prcp, Temp)	Daily (1996 - 2008)
259.2	Gopaghat	Discharge	Daily (1996 - 2008)

Table 3 Detail of selected climate models of fifth phase of the Coupled Model Inter-comparison Project (CMIP5)

CMIP5 Model	Institute	Country	GCM Resolution
ACCESS1-0	Commonwealth Scientific and Industrial Research Organization (CSIRO) and Bureau of Meteorology (BOM)	Australia	1.25° x 1.875°
CCSM4	National Center for Atmospheric Research (NCAR)	USA	0.94° x 1.25°
CNRM-CM5	Centre National de Recherches Me´te´orologiques (CNRM)	France	1.4° x 1.4°
GFDL-CM3	National Oceanic and Atmospheric Administration (NOAA), Geophysical Fluid Dynamics Laboratory (GFDL)	USA	2° x 2.5°
MPI-ESM-LR	Max-Planck-Institut für Meteorologie /Max Planck Institute for Meteorology (MPI-M)	Germany	1.865° x 1.875°
NorESM1-M	Norwegian Climate Centre (NCC)	Norway	1.895° x 2.5°

Table 4 Model performance statistics during calibration and validation under different scenarios considering the time factor

No.	Drainage Area threshold	Time for 1500 simulation (hr.)	Number of sub-basin	HRU	Calibration			Validation		
					NSE	R^2	PBIAS	NSE	R^2	PBIAS
	No elevation band									
1	25K	0.74	7	10 X SB	0.70	0.74	9.8	0.69	0.73	7.40
2	25K	0.45	7	5 X SB	0.61	0.77	37.5	0.63	0.79	36.1
3	25K	0.18	7	1 X SB	0.6	0.77	38	0.61	0.79	36.7
4	10K	5.65	27	10 X SB	0.76	0.82	26.6	0.79	0.86	27.0
5	10K	1.90	27	5 X SB	0.76	0.83	26.0	0.77	0.85	27.4
6	10K	0.5	27	1 X SB	0.77	0.80	17.1	0.77	0.81	18.2
7	2.5K	19.43	73	10 X SB	0.76	0.82	25.0	0.79	0.86	26.5
8	2.5K	10.33	73	5 X SB	0.79	0.82	18.4	0.80	0.85	21.8
9	2.5K	1.51	73	1 X SB	0.77	0.80	16.1	0.77	0.81	17.9
	Maximum elevation band									
10	25K	0.83	7	10 X SB	0.79	0.81	16.0	0.82	0.84	16.8
11	25K	0.43	7	5 X SB	0.79	0.82	15.9	0.82	0.84	16.6
12	25K	0.17	7	1 X SB	0.81	0.83	11.8	0.84	0.84	7.9
13	10K	3.88	27	10 X SB	0.83	0.84	11.0	0.83	0.84	12.1
14	10K	1.99	27	5 X SB	0.83	0.85	12.9	0.83	0.85	12.9

15	10K	0.56	27	1 X SB	0.82	0.84	9.3	0.84	0.84	8.8
16	2.5K	19.61	73	10 X SB	0.82	0.84	10.5	0.83	0.84	12.6
17	2.5K	10.70	73	5 X SB	0.83	0.84	12.3	0.83	0.85	13.4
18	2.5K	1.33	73	1 X SB	0.82	0.84	7.2	0.82	0.83	11.8

Table 5 Explanation of each sensitive SWAT parameter during calibration, with t-Stat, p-value, fitted value, and new minimum and maximum value

Parameter Name	Description	t - Stat	P-value	Rank	Fitted value	New min value	New max value
V__EPCO.hru	Plant uptake compensation factor	-0.09	0.93	35	0.236	0.000	0.564
V__ESCO.hru	Soil evaporation compensation factor	3.95	0.00	13	0.622	0.359	1.000
V__CANMX.hru	Maximum canopy storage	4.74	0.00	9	55.583	27.740	83.260
R__SOL_ALB (...).sol	Moist soil albedo	-1.80	0.07	22	0.152	-0.061	0.216
V__SURLAG.bsn	Surface runoff lag time	0.05	0.96	38	4.013	0.050	5.847
R__CN2.mgt	SCS runoff curve number	22.03	0.00	4	-0.021	-0.254	-0.018
R__SLSUBBSN.hru	Average slope length	-0.85	0.40	31	0.132	-0.117	0.150
R__OV_N.hru	Manning's "n" value for overland flow	-0.38	0.70	32	4.863	4.292	13.881
R__CH_S1.sub	Average slope of tributary channels	-1.26	0.21	26	-0.087	-0.090	0.129
V__CH_N1.sub	Manning's "n" value for the tributary channels	-1.39	0.16	25	0.557	0.343	1.010
R__CH_L1.sub	Longest tributary channel length in subbasin	-0.97	0.33	30	0.261	-0.026	0.321
V__SLSOIL.hru	Slope length for lateral subsurface flow	-7.70	0.00	7	7.379	0.000	78.090
V__LAT_TTIME.hru	Lateral flow travel time	-100.50	0.00	1	16.274	0.000	98.930
R__HRU_SLP.hru	Average slope steepness	2.12	0.03	20	-0.433	-0.456	0.015
V__ALPHA_BF.gw	Base flow alpha factor (days	-1.15	0.25	27	0.629	0.415	1.000
V__GW_DELAY.gw	Groundwater delay (days)	2.93	0.00	15	76.598	34.201	344.799
V__GWQMN.gw	Threshold depth of water in the shallow aquifer required for return flow to occur (mm	-2.65	0.01	16	428.264	101.401	700.599
V__RCHRG_DP.gw	Deep aquifer percolation fraction	2.56	0.01	18	0.523	0.258	0.776
V__REVAPMN.gw	Threshold depth of water in the shallow aquifer for "revap" to occur (mm)	0.12	0.91	34	201.901	139.320	418.080
V__GW_REVAP.gw	Groundwater "revap" coefficient	-1.14	0.26	28	0.108	0.073	0.179
R__SOL_K(..).sol	Saturated hydraulic conductivity	4.66	0.00	10	3.131	1.906	6.719
R__SOL_Z(..).sol	Depth from soil surface to bottom of layer	4.36	0.00	11	1.482	0.212	1.635
R__SOL_AWC(..).sol	Available water capacity of the soil layer	-0.06	0.96	37	0.154	-0.007	0.180
V__ALPHA_BNK.rte	Base flow alpha factor for bank storage	22.64	0.00	3	0.946	0.326	0.980

V__CH_K2.rte	Effective hydraulic conductivity in main channel alluvium	-35.26	0.00	2	42.303	-0.010	258.786
R__CH_S2.rte	Average slope of main channel	2.60	0.01	17	0.047	-0.153	0.082
V__CH_N2.rte	Manning's "n" value for the main channel	-0.09	0.93	36	0.321	0.421	0.300
R__CH_L2.rte	Length of main channel	-4.29	0.00	12	0.045	-0.016	0.351
V__SFTMP.bsn	Snowfall temperature	-7.15	0.00	8	-0.106	-0.130	3.610
V__SMTMP.bsn	Snow melt base temperature	-1.41	0.16	24	-0.013	-1.966	0.678
V__SMFMX.bsn	Maximum melt rate for snow during year (occurs on summer solstice)	0.33	0.74	33	6.145	5.590	8.770
V__SMFMN.bsn	Minimum melt rate for snow during the year (occurs on winter solstice)	2.15	0.03	19	3.733	2.742	4.914
V__TIMP.bsn	Snow pack temperature lag factor	1.59	0.11	23	0.361	0.000	0.638
V__SNOCOVMX.bsn	Minimum snow water content that corresponds to 100% snow cover	3.68	0.00	14	122.512	0.000	317.800
V__SNO50COV.bsn	Snow water equivalent that corresponds to 50% snow cover	-0.01	0.99	39	0.503	0.430	0.890
V__TLAPS (..).sub	Temperature lapse rate (for higher elevation)	10.18	0.00	6	-6.716	-6.290	-7.430
V__PLAPS (..).sub	Precipitation lapse rate (for higher elevation)	15.22	0.00	5	-30.749	-296.300	111.300
V__TLAPS (..).sub	Temperature lapse rate (for lower elevation)	-1.02	0.31	29	-7.477	-7.022	-7.674
V__PLAPS (..).sub	Precipitation lapse rate (for lower elevation)	2.00	0.05	21	54.050	-238.799	253.799
R_Parameter Name = the existing parameter value is multiplied by (1 + a given value)							
V_Parameter Name = replace the existing parameter value by the new value							

Table 6 Model performance during calibration and validation

Objective function value during the model calibration						
Method	p-factor	r-factor	R^2	NSE	RSR	PBIAS
SUFI-2	0.82	0.80	0.84	0.82	0.42	10.5
Objective function value during the model validation						
SUFI-2	0.79	0.72	0.84	0.83	0.42	12.6

Fig. 1. Location map of the West Seti River basin (WSRB) showing river network, and hydro-meteorological stations. Shaded is the topography of the study area.

Fig. 2 Spatial distribution of land use land cover (LULC) within the study area.

Fig.3 Schematic diagram of overall research methodology adopted in this study. DEM: Digital Elevation Model, RCP: Representative Concentration Pathway, HRUs: Hydrological Response Units, RCM: Regional climate Model

Fig.4 Model performance statistics and time required to simulate different scenarios. Red bars represent cases with no elevation band (EB) and blue bars represent EB inclusive cases. SB denotes sub basin and HRU denotes Hydrological Response Unit. NSE, R^2 and PBIAS are model performance metrics.

Fig. 5 Comparison of observed versus 95PPU (95% range of uncertainty) plot of mean daily discharge during the calibration at Gopaghat hydrological monitoring station. The red line shows the best simulated one. NSE and R^2 are model performance metrics.

Fig. 6 Comparison of daily observed and simulated discharge for the calibration period (1999-2005) and validation period (2006-2008) at Gopaghat hydrological monitoring stations. The inverted bar represents basin averaged daily precipitation. NSE and R^2 are model performance metrics.

Fig. 7 Scatter plots of observed versus simulated daily discharge during calibration (left panel) and validation (right panel). The solid lines represent the perfect correlation (R^2 = 1 or y=x), and dashed lines represent the correlation between observed and simulated data.

Fig. 8 Spatial distributions of snow cover areas across the 5 km buffer zone of West Seti River basin for different months. Muhammad and Thapa (2020) improved a raw MODIS 8-day composite product of snow cover and validated with Landsat 8 data. N is the no. of 8-day composite images in the month for the period of 2003 - 2008 and % value indicates the frequency of time snow was observed in that month.

Fig. 9 Temporal variations of a) snow cover area (8-day temporal resolution) across the study area, b) basin-averaged daily maximum temperature (Tmax), daily minimum temperature (Tmin), and daily average temperature [Tavg = (Tmax+Tmin)/2], and c) observed and simulated mean daily discharge at Gopaghat hydrological monitoring stations for the period of 2003 – 2009.

Fig. 10 Inter annual variation of projected annual precipitation across the study area under two warming scenarios: 1) under RCP 4.5 (top panel), and 2) under RCP 8.5 (bottom panel). The solid lines represent the multi model ensemble (MME) of selected climate models and the spreads represent the range of selected climate models. Three selected time periods in our study are F1 (2020-2044), F2 (2045-2069), and F3 (2075-2099).

Fig. 11 Deviation of mean annual precipitation (expressed in %) with respect to the baseline for different future scenarios based on individual climate models and multi model ensemble (MME) of selected climate models. There are two warming scenarios: 1) under RCP 4.5 (blue), and 2) under RCP 8.5 (red) for three time periods (F1: 2020-2044, F2:2045-2069, and F3:2075-2099)

Fig. 12 Inter annual variation of projected annual T_{avg} across the study area under two warming scenarios: 1) under RCP 4.5 (top panel), and 2) under RCP 8.5 (bottom panel). The solid lines represent the multi model ensemble (MME) of selected climate models and the spreads represent the range of selected climate models. Three selected time periods in our study are F1 (2020-2044), F2 (2045-2069), and F3 (2075-2099).

Fig. 13 Deviation of mean annual T_{avg} (expressed in ^{o}C) with respect to the baseline for different future scenarios based on individual climate models and multi model ensemble (MME) of selected climate models. There are two warming scenarios: 1) under RCP 4.5 (blue), and 2) under RCP 8.5 (red) for three future time periods (F1: 2020-2044, F2:2045-2069, and F3:2075-2099)

Fig. 14 Mean monthly precipitation and temperature (T_{max}, T_{min}, and [T_{avg} = (T_{max} + T_{min})/2)]) across the study area of the baseline (dashed), and different future scenarios based on multi model ensemble, MME (solid), and range of selected climate models (respective color spreads). Corresponding labels are depicted in their respective colors. The spreads for T_{max} and T_{min} are not shown. Similarly, T_{max} and T_{min} of the baseline period are also not shown. Left panels are under RCP 4.5 and right panels are under RCP 8.5. Similarly, top two panels are for the F1 (2020-2044) period, middle two panels are for the F2 (2045-2069) period, and bottom tow panels are for the F3 (2075-2099) period.

Fig. 15 Mean monthly river discharge of the baseline (dashed), different future scenarios based on MME (solid), and range of selected climate models (blue spread). Left panels are under RCP 4.5 and right panels are under RCP 8.5. Similarly, top two panels are for the F1 (2020-2044) period, middle two panels are for the F2 (2045-2069) period, and bottom tow panels are for the F3 (2075-2099) period.

Fig. 16 Flow duration curves of mean daily discharge of the baseline and different future scenarios (F1: 2020-2044, F2:2045-2069, and F3:2075-2099) under a) RCP 4.5 and b) RCP 8.5. c) Location of licensed issued hydropower projects in the West Seti River basin, and d) description of licensed issued hydropower projects including capacity of the project in MW obtained from Department of Electricity Development, Government of Nepal.

Fig. 17 Mean annual river discharge of the baseline and different future scenarios in the three future time periods (F1: 2020-2044, F2:2045-2069, and F3:2075-2099) under RCP 4.5 (blue) and RCP 8.5 (red) based on individual climate models and multi model ensemble (MME) of selected climate models.

Fig. 18 Mean seasonal river discharge of the baseline and different future scenarios in the three future time periods (F1: 2020-2044, F2:2045-2069, and F3:2075-2099) under RCP 4.5 (blue) and RCP 8.5 (red) based on multi model ensemble (MME) of selected climate models.

Conflict of interest

No conflict of interest.

Credit Author Statement

All authors conceived and contributed to this study. Bhatta B. and Shrestha P. K. performed the computations. Bhatta B. and Talchabhadel R. contributed to analysis of results and interpretation. Shrestha S. supervised the findings of this study. Bhatta B. wrote the original draft and all authors provided critical feedback and helped shape the research, and manuscript.

Graphical abstract

We used SWAT for hydrological modeling and identified the most sensitive parameters.

Significant improvements were observed when elevation bands were considered.

The projection showed increasing precipitation, temperature and river discharge.

Highlights

- We used SWAT for hydrological modeling and identified the most sensitive parameters.
- Significant improvements were observed when elevation bands were considered.
- The projection showed increasing precipitation, temperature and river discharge.